Technical Challenges Associated with In-Air Wingtip Docking of Aircraft in Forward Flight

Jesse R. Quinlan[1], Jing Pei[2], John R. Cooper[3], Ronald C. Busan[4], Paul M. Rothhaar[5], William E. Milholen II[6]

NASA Langley Research Center, Hampton, VA, 23681

Thomas A. Ozoroski[7], Christopher L. Hartman[8]

Analytical Mechanics Associates, Hampton, VA 23681

Autonomous in-air wingtip docking of aircraft offers significant opportunity for system-level performance gains for numerous aircraft applications. Several of the technical challenges facing wingtip docking of fixed-wing aircraft are addressed in this paper, including: close-proximity aerodynamic coupling; mechanisms and operations for robust docking; and relative state estimation methods. A simulation framework considering the aerodynamics, rigid-body dynamics, and vehicle controls is developed and used to perform docking sensitivity studies for a system of two 5.5% scale NASA Generic Transport Model aircraft. Additionally, proof-of-concept testing of a candidate docking mechanism designed to move the primary wingtip vortex inboard suggests the viability of such an approach for achieving robust docking.

I. Introduction

AERIAL refueling is commonly used to extend the operational range of military aircraft. Modern aerial refueling aircraft systems typically use one of two methods: either a probe and drogue refueling (PDR) system [1] or a boom receptacle refueling (BRR) method [2]. Although the PDR method is a perhaps a simpler approach, the development of an autonomous PDR system for unmanned aerial vehicles (UAVs) has only reached prototype fruition in recent years [3–5]. The BRR method offers some operational advantages but requires a tanker-like vehicle carrying specialized machinery, as well as an additional flight crew member to operate the boom. For military operations, both refueling methods achieve the ultimate goal of range extension; however, both come at a significant operational and design cost in the way of added structures, mechanisms, and flight crew.

An alternative approach to PDR and BRR methods is to physically dock the approaching aircraft wingtip to that of the larger transport aircraft as demonstrated by the U.S. Air Force in Project Tip-Tow in the 1950s [6]. By linking the follower aircraft, an F-84, to each wingtip of the larger bomber transport, a B-29, the entire system of aircraft became more aerodynamically efficient through an effective span increase and subsequent reduction in induced drag. In fact, the system of aircraft was able to fly with the F-84s powered down and with little impact to the range of the B-29. However, achieving this linked configuration proved to be difficult for the pilots due to the proximity aerodynamic effects as the wingtips approached and due to the controls and dynamic sensitivites arising during the engagement. The research demonstrated that in-air wingtip docking of fixed-wing aircraft was indeed feasible; however, the loss of the flight crew in a catastrophic crash as a result of an autopilot malfunction proved that considerable research was still necessary to realize the potential benefits. Hence, these events crystallized the Air Force's path toward the PDR and BRR methods, despite being ultimately a less efficient means of achieving the same range-extending capability.

With the proliferation of low-cost, autonomous, UAV technologies and systems, combined with the advances in physical modeling and simulation across the many disciplines required of aircraft design, the time is right to revisit the technical challenges facing in-air wingtip docking. Furthermore, compelling applications of such a capability are becoming evident. For example, autonomous wingtip docking could ultimately enable low-cost persistent flight platforms for a variety of applications. Of particular interest are high-altitude long endurance (HALE) applications,

---

where conventional refueling is made difficult due to the flight altitudes and structurally-flexible nature of the airframes and for which missions may require month- or year-long endurance [7]. By launching aircraft independently from conventional runways and physically docking wingtip-to-wingtip at or near cruising altitude, designers may finally realize a way to reliably operate HALE vehicles for ultra-long endurance. With the ability to dock and undock in-air, additional aircraft could be launched to altitude to replace the wingtip mounted aircraft with additional fuel or batteries to keep the primary payload at altitude persistently. Hence, the development of a HALE aircraft for persistence is the ultimate objective of the work presented in this paper toward autonomous, in-air, wingtip docking.

In order for autonomous in-air wingtip docking to become feasible, several technical challenges must be addressed. Specifically, demonstrating a robust docking concept-of-operations (CONOPS) requires investigation in several key areas, including: high-fidelity modeling of the aerodynamic coupling that occurs at close proximity; high-fidelity dynamics and controls modeling in order to perform sensitivity studies on vehicle design parameters to ensure safe and reliable docking; and devising the sensor suite and state estimation methods necessary to accurately construct relative state data. The current paper presents recent work toward each of these three critical challenges.

This paper is organized as follows. In Section II, the CONOPS devised for an initial docking demonstration is presented, which sets forth assumptions and constraints on the modeling and simulation efforts. In Section III, work toward the three technical challenges determined to be in the critical path of realizing feasibility of autonomous in-air wingtip docking of fixed-wing aircraft is presented, where: investigations into the proximity aerodynamics are described in Section III.A; a candidate linkage mechanism concept and associated operational considerations are described in Section III.B; and a study into the onboard sensors and state estimation algorithms required to accurately compute relative state data is presented in Section III.C. The work shown in Section III is then leveraged in Section IV to perform simulations of two baseline aircraft autonomously docking in-air wingtip-to-wingtip. Specifically, approach and docking trajectory simulations and dynamics sensitivity studies are presented in Section IV.A, and proof-of-concept testing of the docking mechanism described in Section III.B is presented in Section IV.B.

II. Docking Demonstration Concept-of-Operations

This section provides a high-level overview of the docking CONOPS, representative guidance, navigation, and controls (GN&C) requirements, and baseline trajectory design for the initial technology demonstration. The system consists of a *Target* aircraft and a *Chaser* aircraft. The mission contains three main phases. The first is a Rendezvous and Formation Flying phase, where the Chaser starts out somewhere below, behind, and away from the Target aircraft and follows a pre-planned trajectory towards the desired Formation Flying Target (FFT) point. Once it reaches the FFT point, the Chaser would subsequently perform a series of formation flying experiments to characterize the performance of the navigation and control subsystems. The second phase is a Proximity Operations phase, which starts upon successful completion of the first phase. Here, the wingtip of the Chaser aircraft is within the wake influence of the Target and both vehicles begin to experience the effects of proximity aerodynamics. The Chaser would then slowly maneuver itself towards the Target aircraft to reduce the wingtip-to-wingtip separation distance. The third and final phase is the Linking phase, which begins once the two wingtips are within the physical capture volume of the docking mechanism. During this phase, the aircraft are expected to maintain constant wingtip-to-wingtip relative separation while the linking mechanism completes the latching and linking of the two wingtips. Figure 1 is a schematic showing all three phases of the mission; the proximity operations and linking phases are represented in the dashed box.
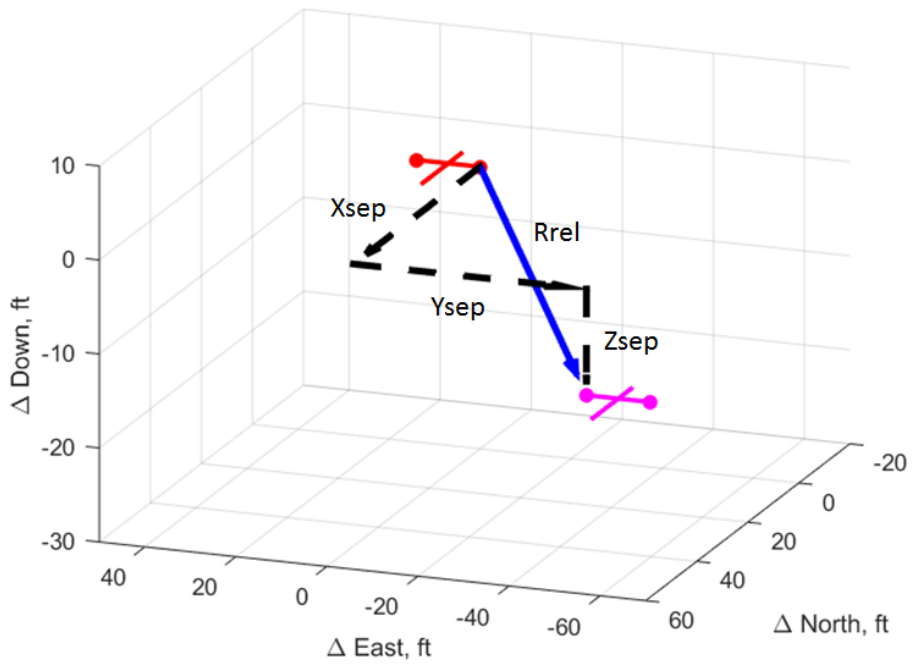
In this CONOPS, the Chaser is expected to perform all the necessary manueuvers while the Target aircraft maintains a straight, steady-level flight. In discussing the relative positional states of the vehicles, a local moving reference frame with respect to the wingtip of the Target is adopted. The relative position vector, R_{rel}, and its components, longitudinal (X_{sep}), lateral (Y_{sep}), and vertical (Z_{sep}) separations, are shown in Fig. 2.

A. Rendezvous and Formation Flying

The Rendezvous phase begins with the Chaser at a safe distance behind, below, and away from the Target. The Chaser would maneuver itself along a pre-planned trajectory towards the FFT point. The preliminary FFT point is choosen to be $X_{sep} = 0$ ft, $Y_{sep} = $ -30 ft, $Z_{sep} = 0$ ft, such that the Chaser is parallel to the Target with a 30 ft standoff distance from wingtip-to-wingtip. Wake interference aerodynamics are assumed to become significant at a distance that is closer than the FFT point. For precautionary reasons, a requirement on the trajectory design is that the Chaser shall not fly within the wake of the Target aircraft during the Rendezvous phase. A description of the analytical wake model used in this study is provided in Section III.A. Furthermore, the approach velocity towards the FFT point shall not exceed 2 ft/s at any point in the Rendezvous phase.

2
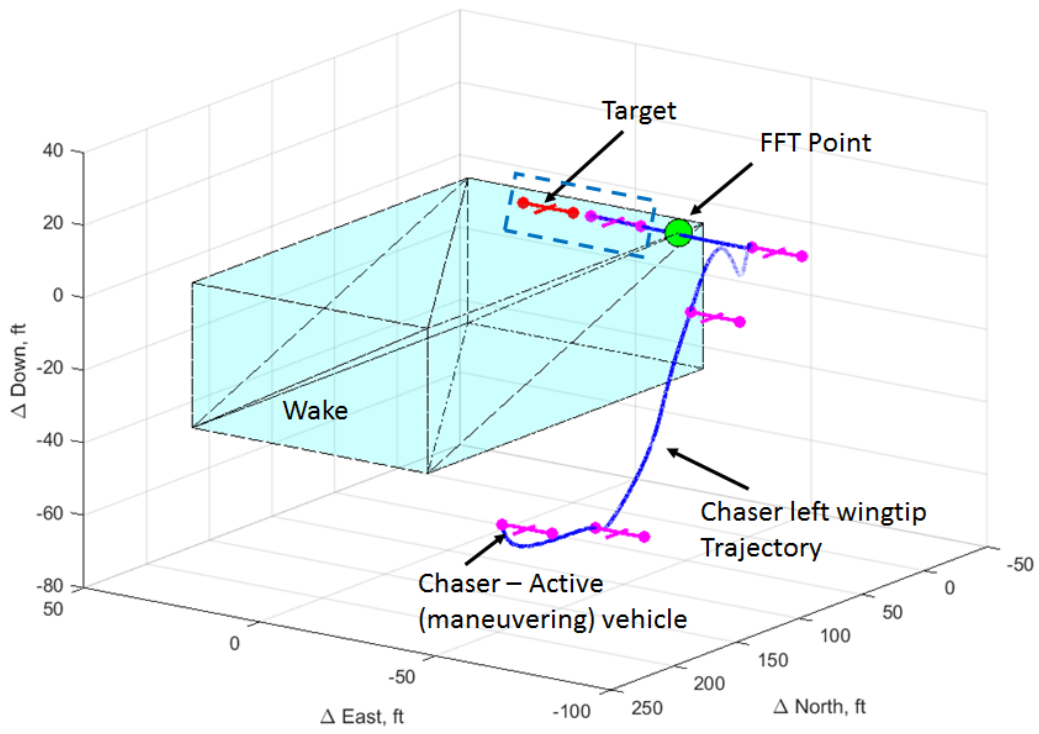
Fig. 1   Concept-of-Operations illustration depicting the three main phases.

Fig. 2   Coordinate system convention.

Once the Chaser has reached the FFT point, a series of precise formation flight experiments is scheduled to characterize the performance of the navigation and control subsystems. The Chaser is expected to hold constant position for at least 60 seconds with an error bound of 1.5 ft in magnitude. Figure 3 depicts the formation flight positional requirement as a sphere with a radius of 1.5 ft. In addition, the relative velocity error shall not exceed 0.1 ft/s in any axis throughout the formation flight phase. Table 1 provides notional GN&C requirements during the Rendezvous and Formation Flying phase. Violation of any of the formation flight requirements would trigger an abort manueuver.
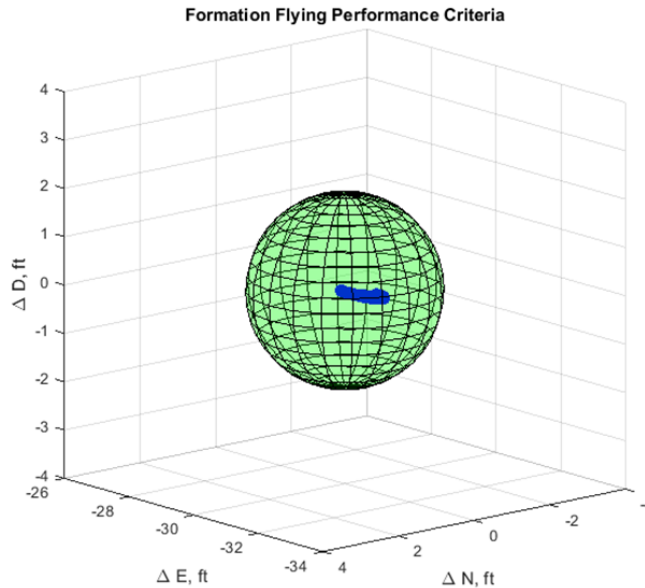
Fig. 3   Formation flight position error requirement depicted by a shaded spere.

Table 1   Representative Formation Flying Requirements

Formation Flight Metrics	units	values
Maximum Approach Velocity	ft/s	2
Formation Flight Duration	s	60
Formation Flight Standoff Distance	ft	[0 -30 0]
Formation Flight Relative Position Error	ft	1.5 (each axis)
Formation Flight Relative Velocity Error	ft/s	0.1 (each axis)
Target Vehicle Roll/Heading Angles	deg	2

B. Proximity Operations

The proximity operations phase starts once the Chaser successfully executes the Formation Flying phase. The current approach trajectory depicted in Fig. 1 shows a pure translation along Y_{sep} where a bank angle command is issued to the Chaser. This is merely a placeholder and is subject to change depending on the final design of the linking mechanism. In order to mitigate the risk of collision in this region dominated by proximity aerodynamics, the Chaser is to slowly manuever its way towards the Target with a nominal velocity of 0.05 ft/s along Y_{sep}. In addition, tight error bounds on the relative velocities and positions are placed on the Chaser vehicle. Figure 4 shows the nominal approach trajectory along with the approach corridor. Table 2 provides notional GN&C requirements for the Proximity Operations phase. These requirements are a direct reflection of the precision and accuracy of the sensors and actuators, time delays in the system, and robustness of the control laws to uncertain dynamics. Violation in any of these approach corridor

requirements would trigger an abort maneuver.
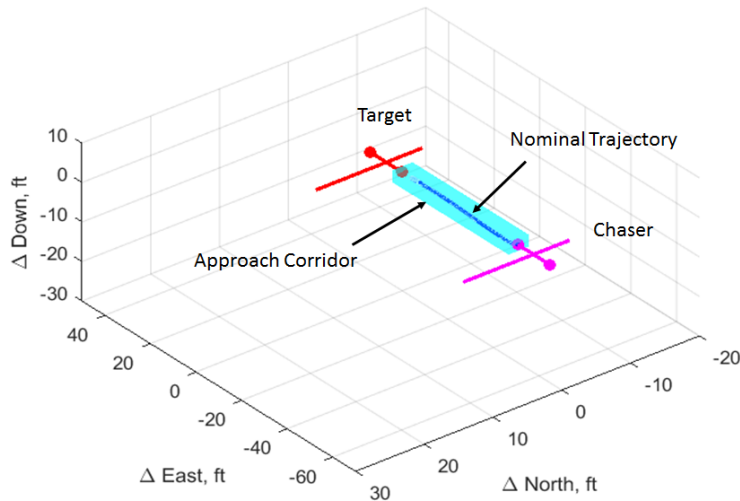
Fig. 4   Proximity operations schematic illustrating approach corridor and nominal trajectory for the Chaser aircraft as it approaches the Target aircraft.

**Table 2   Representative Proximity Operations Requirements**

Proximity Operations Metric	units	values
Nominal Approach Velocity in Y_{sep}	ft/s	0.05
Approach Velocity Error	ft/s	0.05
Relative Velocity Error in X_{sep} and Z_{sep}	ft/s	0.05
Relative Position Error Corridor in X_{sep} and Z_{sep}	ft	1
Target Vehicle Roll/Heading Angles	deg	2

C. Linking

The Linking phase starts once the wingtip of the Chaser is within the physical capture volume of the linking mechanism. The capture state-space is defined as the set of relative states (position, velocity, attitude, attitude rates) for which the linking mechanism can successfully latch the two wingtips together. During the linking process, the Chaser is to hold a constant relative position with minimal residuals in relative velocity, attitude, and attitude rates. As a result, the 12-dimensional hypersurface used to define the capture state-space can be reduced down to three dimensions consisting of only the relative position states. Due to the lack of maturity in design of the linking mechanism, the physical capture volume is currently modeled as a sphere with a radius of 0.5 ft, as shown in Fig. 5. Table 3 provides notional GN&C requirements for the Linking phase. Upon successful completion of the Linking phase, the mode of operation immediately switches to that of a single aircraft.

III. Technical Challenges Associated with Wingtip Docking

In order to simulate the CONOPS described in the previous section, the proximity aerodynamic effects, designing a robust linking mechanism, and sensor and state estimation challenges referenced in Section I were investigated. Though the configuration is not designed for in-air docking, the 5.5% scale NASA Generic Transport Model (GTM) aircraft was used for the model and simulation development in this study due to the relatively well-documented body of work surrounding the aircraft [8]. Once benchmarked using the GTM, future conceptual design studies targeting in-air docking will leverage these tools and methods. In Section III.A, a comparative study of aerodynamic modeling approaches for
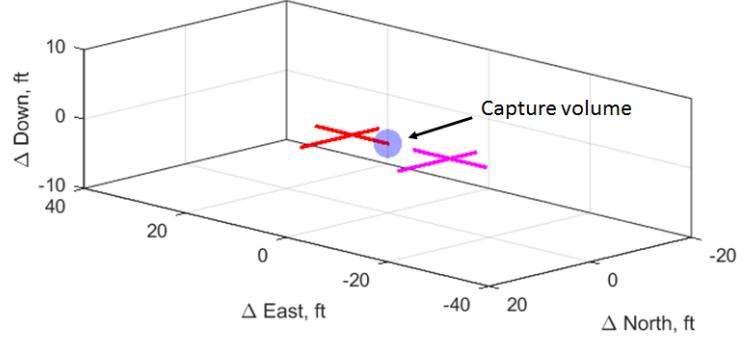
Fig. 5 Linking phase schematic illustrating the required physical capture volume at the wingtip of the Target aircraft by the shaded sphere.

Table 3   Representative Linking Requirements

Linking Metric	units	values
Relative Velocity Error (3 axis)	ft/s	0.05
Relative Position Error (3 axis)	ft	0.5
Target Vehicle Roll/Heading Angles	deg	2

two 5.5% GTM aircraft approaching wingtip-to-wingtip is presented. In Section III.B, a candidate docking mechanism is presented, and contributing factors to its design and operation are discussed. Finally in Section III.C, a candidate sensor package and state estimation approach is discussed for application to a subscale flight demonstation of autonomous wingtip docking.

A. Proximity Aerodynamics

In this section, two methods for analyzing the aerodynamic interactions between aircraft in close proximity are compared. The first method is an approach combining the Generic Nonlinear Aerodynamic (GNA) model for the GTM [9] with the NASA-Burnham-Hallock model for computing three-dimensional wake velocity fields around the wingtips [10]. The second approach is Euler simulations of the proximity aerodynamics using the Cart3D computational fluid dynamics (CFD) solver [11], in which solutions were computed as a function of wingtip setoff-distance for two GTM aircraft.

1. NASA Burnham-Hallock Model

The NASA-Burnham-Hallock Model provides a three-dimensional wake velocity field around the wingtips. The model is defined as follows:

$$
\begin{aligned}
W_{wake}(x,y,z) &= -W_r(x,y,z) + W_l(x,y,z) \\
W_r(x,y,z) &= \frac{\Gamma}{4\pi} \frac{y-b/2}{(y-b/2)^2 + z^2 + r_c^2} \left[1 - \frac{x}{\sqrt{x^2 + (y-b/2)^2 + z^2}}\right] \\
W_l(x,y,z) &= \frac{\Gamma}{4\pi} \frac{y+b/2}{(y+b/2)^2 + z^2 + r_c^2} \left[1 - \frac{x}{\sqrt{x^2 + (y+b/2)^2 + z^2}}\right] \\
V_{wake}(x,y,z) &= -V_r(x,y,z) + V_l(x,y,z) \\
V_r(x,y,z) &= \frac{\Gamma}{4\pi} \frac{-z}{(y-b/2)^2 + z^2 + r_c^2} \left[1 - \frac{x}{\sqrt{x^2 + (y-b/2)^2 + z^2}}\right] \\
V_l(x,y,z) &= \frac{\Gamma}{4\pi} \frac{-z}{(y+b/2)^2 + z^2 + r_c^2} \left[1 - \frac{x}{\sqrt{x^2 + (y+b/2)^2 + z^2}}\right]
\end{aligned}
\tag{1}
$$

6

where W and V are the downwash and sidewash velocity components respectively, the subscripts r and l denote contributions from the left and right wingtips respectively, x, y, and z are Cartesian coordinates in the vehicle's body-centered reference frame, r_c is the core radius of the vortex, b is the wing span, and

$$\Gamma = \frac{4mg}{\rho V \pi b} \tag{2}$$

where ρ is the air density, V is the free-stream velocity, m is the vehicle mass, and g is the graviational acceleration. An approximation of overall wake-induced velocity experienced by aircraft i is established as the average of three points along the wingspan. For this calculation, consider points at each wingtip and at the center of gravity of the vehicle. Then the total wake-induced velocity field is given by

$$\begin{bmatrix} u_{wake} \\ v_{wake} \\ w_{wake} \end{bmatrix} = \sum_{j=1, j \neq i}^{n} R_{B_j}^{B_i} \begin{bmatrix} 0 \\ \frac{V_{wake_j}(x_{LW}, y_{LW}, z_{LW}) + V_{wake_j}(x_{RW}, y_{RW}, z_{RW}) + V_{wake_j}(x_{CG}, y_{CG}, z_{CG})}{3} \\ \frac{W_{wake_j}(x_{LW}, y_{LW}, z_{LW}) + W_{wake_j}(x_{RW}, y_{RW}, z_{RW}) + W_{wake_j}(x_{CG}, y_{CG}, z_{CG})}{3} \end{bmatrix} \tag{3}$$

where $R_{B_j}^{B_i}$ is the rotation matrix from the j body frame to the i body frame, the subscripts LW and RW denote the left and right wingtips respectively, CG denotes the center of gravity, and n is the number of vehicles in the system. For the current paper, $n = 2$, for the Chaser and Target aircraft system. By combining the NASA-Burnham-Hallock model for proximity aerodynamic contributions with those of the independent aircraft via the GNA method, this approach is used to simulate the aerodynamics of the system of aircraft.

Figure 6 shows a cross-section of the wake velocity field induced by wingtip vortices of a single aircraft according to the NASA-Burnham-Hallock model. Figure 7 shows the resulting velocity field when two vehicles come in close proximity of each other. It can be seen that the upwash in between the wingtips increases, which results in rolling moments on both vehicles that must be overcome by the inner-loop controllers.

While the NASA-Burnham-Hallock model offers a rapid means of estimating the aerodynamic coupling of proximal aircraft, the model requires the user to specify the vortex core radius, r_c. Trades on r_c suggest the net aerodynamic coupling effect is sensitive to this parameter. For example, a doubling of the r_c from $0.1b$ to $0.2b$ results in more than a doubling of lift coefficient, C_L, induced on the follower aircraft from the aerodynamic coupling, which is shown in Fig. 8. Further, the model is somewhat ill-defined as the separation distance approaches zero (i.e. linked), as the definition of the wingspan effectively changes once the aircraft become a single linked configuration.

2. Cart3D Simulations

Although the GNA and NASA-Burnham-Hallock models offer computational speed, the approach requires specifying model parameters, such as the vortex core radius, r_c, which are likely not known *a priori* and also relies on a simplified representation of the velocity field induced by the wingtip vortex. In order to gauge the accuracy of this approach and to further investigate the aerodynamic interactions that occur at close proximity, Euler simulations were performed for a wide range of Chaser and Target setoff-distances using Cart3D.

The baseline GTM surface geometry is shown in Fig. 9, with the underwing nacelles and pylons removed for simplicity. This geometry is a 5.5% scale version of the full GTM geometry, with a wingspan of approximately 82.0 inches and a total length of approximately 102.5 inches. After triangulating the surface geometry of the baseline GTM, a mesh convergence study was performed to confirm the production surface and associated volume mesh was satisfactory, relative to integrated aerodynamic loads; the baseline, single aircraft, production surface and volume meshes contained 1.5 million triangles and 0.6 million hex cells, respectively. A baseline verification simulation was performed initially with a single GTM aircraft at an angle-of-attack of $4.5°$, freestream velocity of 125 ft/s, and altitude of 1200 ft; a standard atmosphere model was assumed [12]. Comparisons of the GNA model to the CFD solution showed significant error in the predicted lift and drag, and after considerable investigation, the authors determined the error to be predominantly associated with two sources. The first source of error was due to the vehicle model being untrimmed (i.e. the elevator remained undeflected). The second source was related to the inviscid solver's ability to model low Mach number applications. Because the ultimate objective of this study was to investigate the trends associated with aerodynamic coupling for systems of aircraft, the baseline model was calibrated to the GNA model lift and drag coefficient, C_L and C_D, respectively, by increasing the simulated Mach number. At the simulated condition of Mach 0.3, the flow was still effectively incompressible, yet C_L and C_D agreed with those predicted by the GNA Model to within 10%.
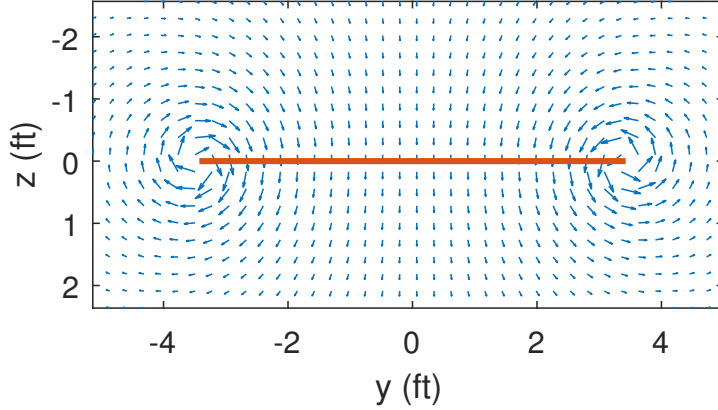
**Fig. 6   Cross-section of wake-induced velocity flow field at $x = 0$. The red line represents the wing.**
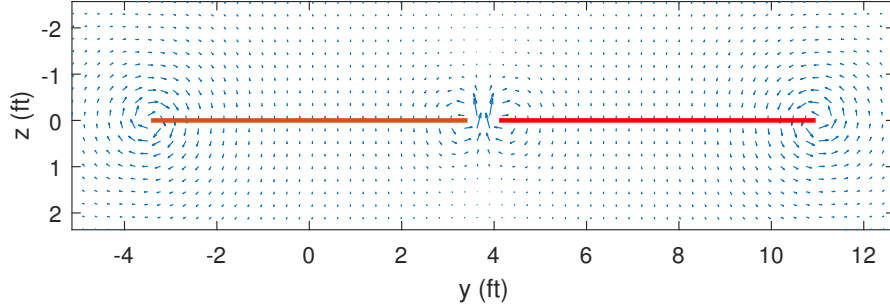
Fig. 7   Cross-section of wake-induced velocity flow field at $x = 0$ for two vehicles in close proximity. The red lines represents the two wings.

The baseline GTM surface mesh and nominal flight conditions were then used to perform a trade study investigating the aerodynamic coupling associated with flying two GTM aircraft docked wingtip-to-wingtip and at close proximity. Simulations of this system of two GTM aircraft were performed as a function of setoff-distance in the three Carteision directions. The setoff-distance state space ranged from docked to approximately one wingspan distance in each of the three Cartesian dimensions, and simulations were performed at 8 logarithmically distributed points ranging from 10^{-3} to 10^2 inches in each of the three setoff directions resulting in 512 independent flow solutions. Each simulation reached convergence in L_2-norm of the density residual and integrated forces. To facilitate the automation of the volume meshes, the docked configuration required a small distance between the two wingtips, which was set to 10^{-3} inches. This small distance permitted the creation of volume cells between the wingtips, while still effectively simulating a docked configuration. Surface contours of pressure coefficient are presented in Fig. 10 for one such *docked* solution, showing the entire configuration in (a) and the wingtip region in (b).

The trends observed in these Cart3D flow solutions agreed well with those of previous investigations [13], as well as the NASA-Burnham-Hallock model. The C_L and C_D were extracted for $Z_{sep} = 10^{-3} in$ and plotted in the X_{sep}-Y_{sep} plane for each of the Target and Chaser aircraft in Fig. 11; note that a cubic interpolation was performed on the discrete data points to render these surface plots. These plots show clearly that the most aerodynamically advantageous position of the aircraft is that of a docked configuration, where the C_L reaches a global maximum for both the Target and Chaser aircraft and where C_D reaches a global minimum for the Target aircraft. Interestingly, the Chaser aircraft achieves a minimum C_D at some distance behind the Target, in the streamwise direction, and just off the wingtip, in the spanwise direction. While this minimum point is quite comparable to the docked C_D, there may be some interesting interplay of the wake and wingtip vortex from the Target that results in this small apparent gain in Chaser drag performance.

(a) Vortex core radius of $0.1b$

(b) Vortex core radius of $0.2b$
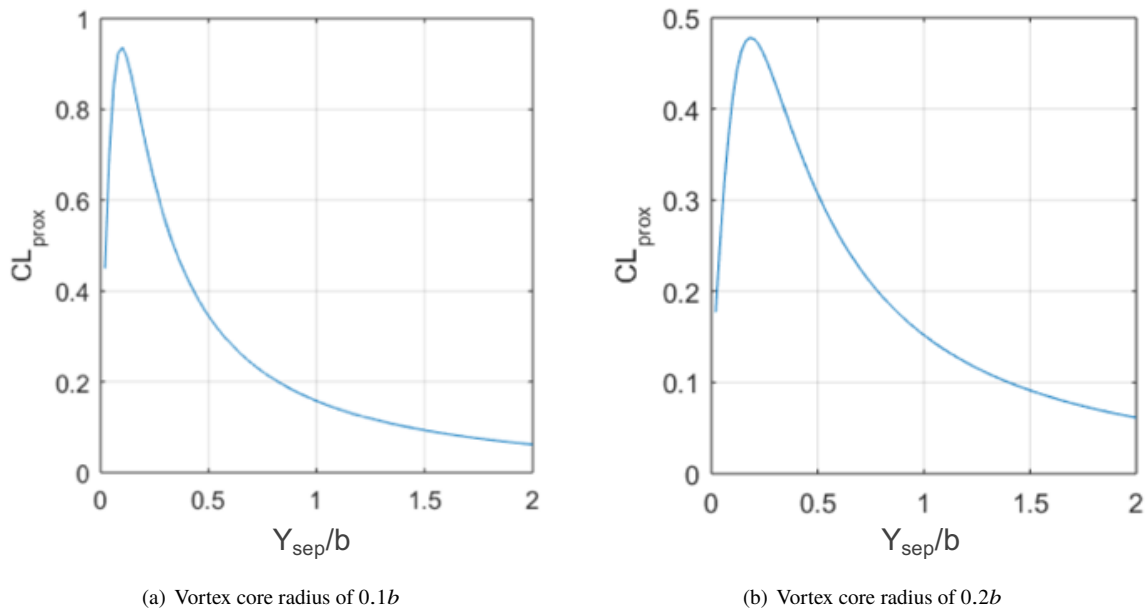
Fig. 8   Proximity lift coefficient, $C_{L_{prox}}$, for the Chaser as a result of aerodynamic coupling with the Target and as a function of separation distance normalized by wing span, Y_{sep}/b, in the spanwise direction for two vortex core radii.
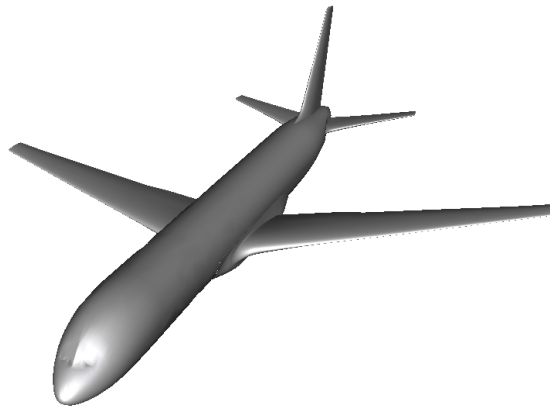

Fig. 9   Solid model geometry of the GTM aircraft with nacelles and pylons removed.

Another interesting observation involves the C_L performance for the Target and Chaser aircraft. Specifically, in Fig. 11, one can see that C_L gains persist for the Follower aircraft even at X_{sep} distances approaching 100 in. This result should not be surprising, as the wingtip vortex being shed from the Target aircraft continues to influence the Chaser for several body lengths behind the vehicle, as has been demonstrated routinely in studies of formation flight. The C_L benefit does, however, drop off similarly to that of the Target aircraft in the spanwise offset direction, though, as expected.

Similarly to the lift and drag, the roll (C_l), pitch (C_m), and yaw (C_n) moment coefficients were also investigated, and similar surface plots for these parameters are shown in Fig. 12. Again, these parameters are plotted for both the Target and Chaser aircraft, and the surface plots were rendered using a cubic interpolation of the underlying discrete data. Inspecting the roll coefficients confirms the expected aerodynamic coupling trends; that is, in a docked configuration, the aircraft tend to roll away from each other, as shown by the Target and Chaser aircraft each achieving the maximum
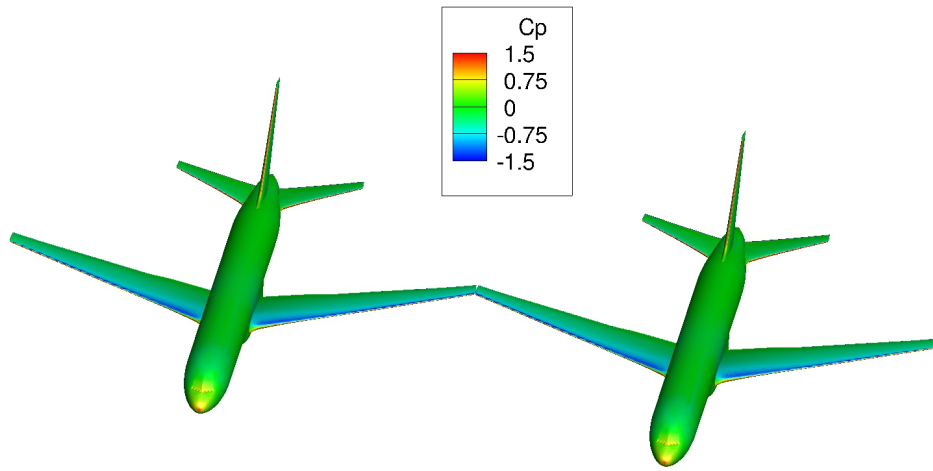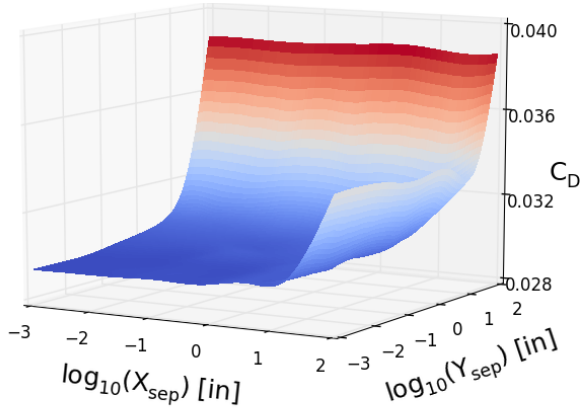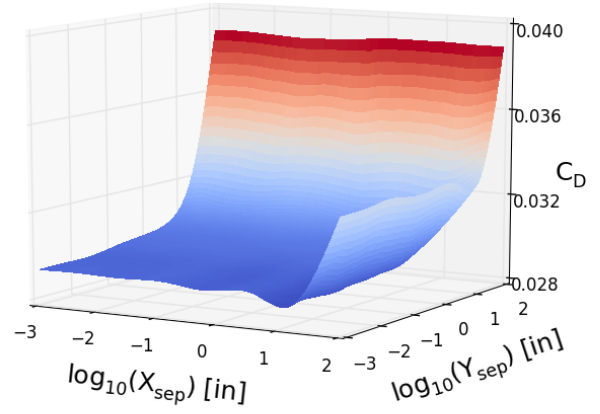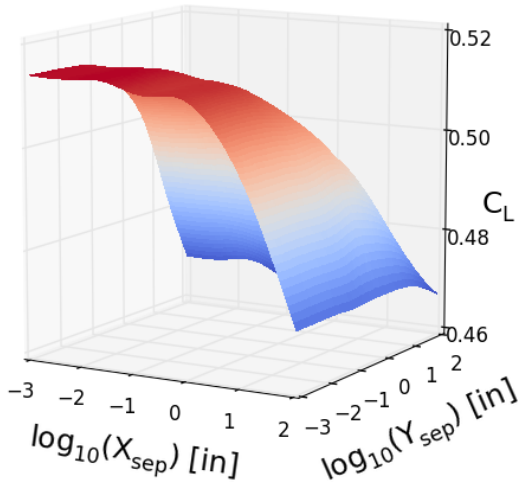
(a) Two-aircraft configuration.
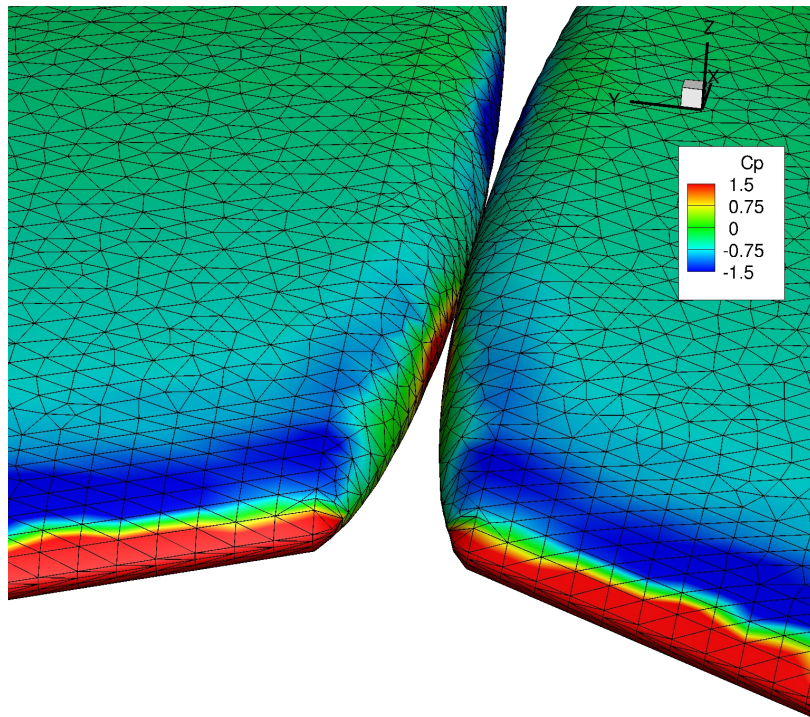
(b) Wingtip region.

Fig. 10   Surface contours of pressure coefficient for two GTM aircraft models in a very-near proximity configuration.
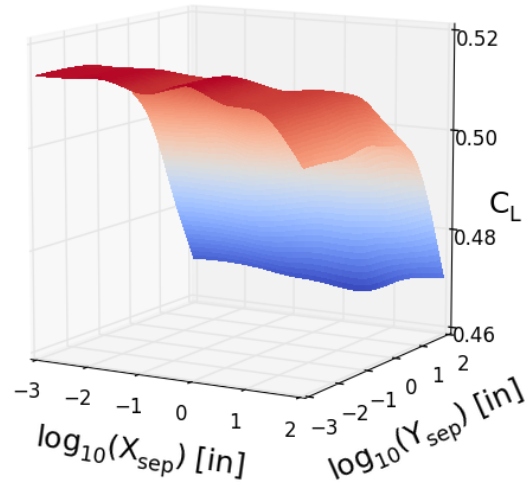
(a) Drag coefficient for the Target aircraft.

(b) Drag coefficient for the Chaser aircraft.

(c) Lift coefficient for the Target aircraft.

(d) Lift coefficient for the Chaser aircraft.

Fig. 11   Cart3D simulation lift and drag coefficient solutions in X_{sep}-Y_{sep} space at $Z_{sep} = 10^{-3} in$.

magnitude C_l at the minimal offset distances. Further, as C_L is increased approaching the linked configuration, the aircraft respond by tending to pitch up because these models were not aerodynamically trimmed. Finally, investigating the yaw behavior as a function of offset distance confirms the general tendency to yaw in opposite directions, away from each other due to the wing vortex interactions. Note that the C_n data varies less than one order of magnitude, compared to C_l and C_m, and that these surface plots exhibit more local variation across the investigated X_{sep}-Y_{sep} space. Since the mesh convergence study was done using C_L and C_D as the objective function and due to the relatively small order of the C_n values, the error associated with the geometry, meshing, and solver may be producing some of the local variation seen in these plots. However, despite this potential error, the general trend in C_n agrees with theory, in that at the smallest offset distances, the aircraft tend to yaw away from each other, and that this coupling diminishes at the largest offset distances.

## B. Robust Docking Operations

In order to ensure high probabilities of success for the docking CONOPS laid out in Section II, the Target and Chaser aircraft must employ linkage mechanisms designed to account for the uncertainties associated with the vehicle system dynamics, aerodynamics, and aeroelastic behavior. To this end, a variety of operational concepts were considered for achieving robust docking, including: reducing the unsteady aerodynamics associated with wingtip vortices interacting, increasing the physical capture volume in which successful docking can occur, and increasing the deflections or misalignments that can be handled by the docked wingtips.

Experience from previous bomber-fighter docking programs, such as Project Tip-Tow, demonstrated the need to minimize the unsteady interactions of the aircraft wingtip vortices during the docking maneuver. The use of extendible booms that pushed the linking hardware outside of the wingtip vortex of the bomber was successfully demonstrated, but this approach required additional structural weight that would likely be unsuitable for a HALE configuration. Therefore, an alternate concept to achieve the same aerodynamic effect without increasing structural weight was developed, which relies on the assumption that the wingtip vortices can be repositioned through intelligent modifications to the wing lift distribution with the use of distributed control surfaces.

If the wings of the Target and Chaser aircraft each have multiple trailing control surfaces across the semispan, the control surfaces nearest the tip can be deflected to nullify the lift in this outboard section of the wing. This modified lift distribution effectively turns the most outboard sections of the wing into a faired, non-lift-producing boom during the docking operation - allowing the wingtips to get very close to each other in flow that is free from major wingtip vortex interactions. The temporary loss of lift associated with this operation can be compensated by increasing lift further inboard on the wings or by allowing the aircraft to descend during the docking maneuver. Since multiple spanwise trailing edge control surfaces are likely required for HALE aircraft wings to enable maneuvering and stability, the use of the proposed concept to reduce wingtip vortex interactions during docking will not impose significant additional structural weight in the way that the bomber-fighter booms would.

Whereas PDR and BRR refueling typically require highly-precise flight control to achieve the mechanical link between the aircraft, the authors explored various options to increase the size of the physical capture volume defining how close the wingtips of the aircraft have to be to successfully dock. Several military development programs employ hook and cable capture techniques to recover UAVs [14, 15]. Figure 13 shows a modification of this concept applied to proposed wingtip docking, where one aircraft has a lightweight cable extending out from its wingtip and the other aircraft has a hook near its wingtip. A small drogue bulb at the end of the cable helps stabilize the trailing cable position through a combination of inertial and aerodynamic drag forces. When the aircraft with the wingtip hook makes contact with the cable on the outboard portion of its wing, the hook engages the cable, which will have a simple capture cam. Once the cable is captured by the hook, the other aircraft retracts the cable and pulls the wingtips together to complete the docking maneuver.

Rigid wingtip connections would require significant structure to counteract forces and moments in all directions, which would then need to be carried through the wings. An alternate approach, which has been successfully applied to aerodynamic skirts on high speed trains, is to allow the joints enough flexibility so that transient loads do not introduce large forces in the primary structure. Hence, there is some perceived value in initially looking at semi-rigid or partially-compliant wingtip docking joints. A combination of cable connections and flexible material at the wingtip joints will restrain against relative translation and large rotations while also allowing for some angular misalignment and movement. Since each component aircraft of the assembled configuration will be generating its own lift and control forces, it is not necessary for the wingtip joints to *carry* the docked aircraft; rather, docking itself provides significant aerostructural benefit by distributing inertial loadings and preventing extreme wing structure deflections.
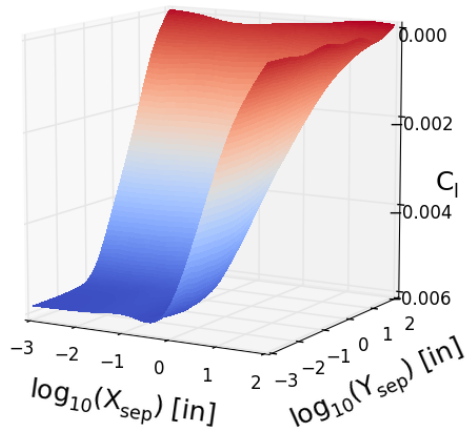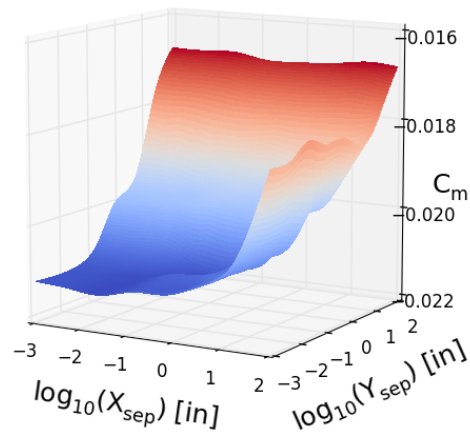
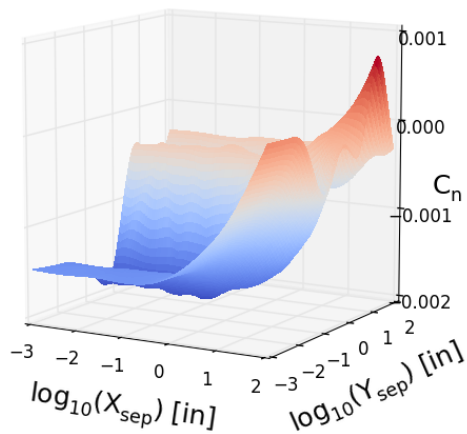(a) Rolling coefficient for the Target aircraft.
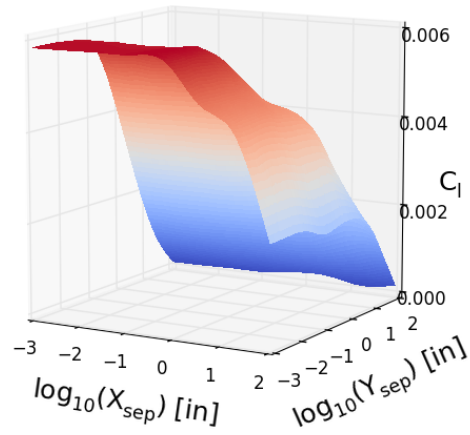
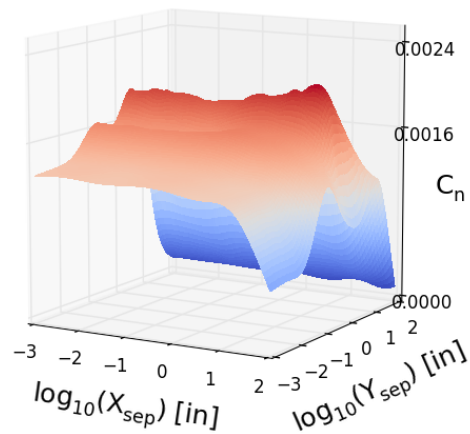(b) Rolling coefficient for the Chaser aircraft.
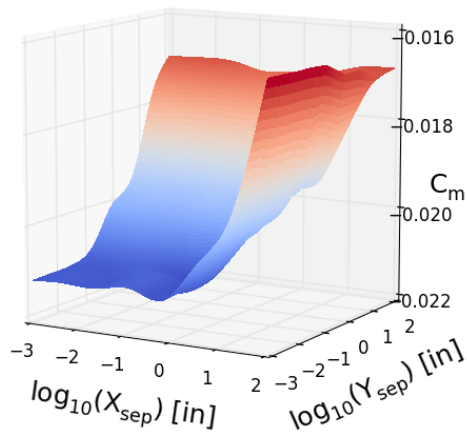
(c) Pitching coefficient for the Target aircraft.

(d) Pitching coefficient for the Chaser aircraft.
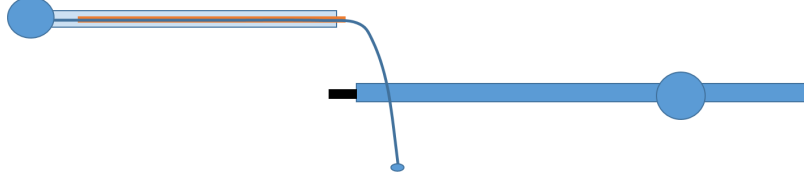
(e) Yawing coefficient for the Target aircraft.

(f) Yawing coefficient for the Chaser aircraft.

Fig. 12   Cart3D simulation roll, pitch, and yaw coefficient solutions in X_{sep}-Y_{sep} space at $Z_{sep} = 10^{-3} in$.

Fig. 13   Linking mechanism concept based on hooking trailing cable.

Table 4   Sensor Suite

| GN&C Sensors	Functionality
IMU Gyroscope	Inertial attitude and rate estimation
IMU Accelerometer	Inertial position and velocity estimation
Carrier Phase GPS (CDGPS)	Relative position and velocity estimation
Linking Camera	Relative position estimation for linking

C. Sensor Suite

To perform the multitude of GN&C functions required during Rendezvous, Formation Flight, Proximity Operations, and Linking, a set of GN&C sensors is selected. Table 4 outlines the candidate sensors along with their functionalities. Due to size constraints, cost, and simplicity considerations, carrier phase differential global positioning system (CDGPS) is chosen as the primary relative navigation sensor between the Target and Chaser. Depending on the final design of the linking mechanism a camera may be required for the Linking phase. CDGPS [16, 17] provides a few-centimeter relative positioning accuracy when a real time kinematic (RTK) solution or a lock have been achieved between two units. CDGPS was recently used for NASA's On-orbit Autonomous Assembly of NanoSatellite (OAAN) [18] ground demonstration. A pair of units is required to obtain a relative navigation solution between the two phase centers of the GPS antenna in the local North-East-Down (NED) frame.

The Swift Navigation Piksi [19], the commercial CDGPS hardware used for OAAN, is selected as the baseline for this effort. Data obtained by the Piksi includes several error sources. The first is random noise, for which the error is driven by a stochastic process and changes for each measurement. In the navigation software the noise is smoothed with a Kalman filter (assumes Gaussian distribution). The second error source is bias error from GPS satellite constellation geometry. Docking success is sensitive to this slow moving stochastic error and tests indicate that this error could be as large as a few centimeters. The third error source is associated with incorrect Integer Ambiguity Problem (IAP) solutions, and this error can range from a few centimeters to tens of meters in relative position. It can occur suddenly during operation or arise during initialization of the Piksi hardware. Due to its rare occurrence, it is not considered part of the nominal operational scenario. Extensive static testing has been performed to obtain an initial estimate of the measurement noise covariance and bias error.

Figure 14 is a sample data set from a static test showing the east component of the NED relative position vector. Tests were performed in an open field free of obstacles to eliminate any errors due to multipath. The true distance was determined via a tape measure (153.5 cm), the blue dots are the measurements, and the red line is the weighted average. It is apparent from this plot that there are two noise components: 1) white noise, 2) slow moving stochastic bias. The residuals between the running average fit line and actual data points were used to determine the white noise. The amplitude of the running average fit line away from the true value represents the stochastic bias. Both of these parameters have means close to zero, and the bias is slow moving. To measure the stability of the bias, the mean and the standard deviation of the absolute value of the change in the amplitude is computed at each time step, which is selected as 25 seconds. Table 5 tabulates the standard deviations of the white noise and the bias stability. The errors (bias and noise) are largest in the Down direction, which is consistent with manufacturer specifications.

Figure 15 is a representative model of the Piksi error used in the simulation. The model consists of two sources of noise: 1) slow varying stochastic noise (red line) about the mean (green line); and 2) white noise (blue dots) about the red line. The stochastic noise model had a time constant of 25 seconds. The bias model keeps track of a cumulative probability density function of the moving average line given the bias error; therefore, if the bias creeps towards the thresholds (+/-6 cm), then the tendency for it to keep growing in that direction reduces proportionally. At any time step, the movement of the moving average line is sized by a distribution based on the stability parameters. The model can be
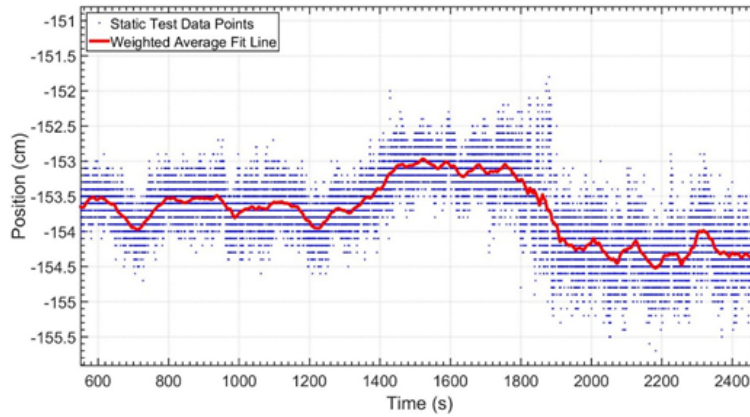
Fig. 14 **Sample static test of Piksi hardware, where measurements are shown (blue dots) around the weighted average (red line).**

Table 5 **CDGPS Error Parameters from Static Tests 1σ**

Error Type	North	East	Down
White Noise (cm)	0.43	0.325	0.87
Bias Stability (cm/time step)	0.48	0.36	0.96

also be scaled by a gain factor or the time constant can be increased to affect the variability of the error signal and used during dispersion analysis.
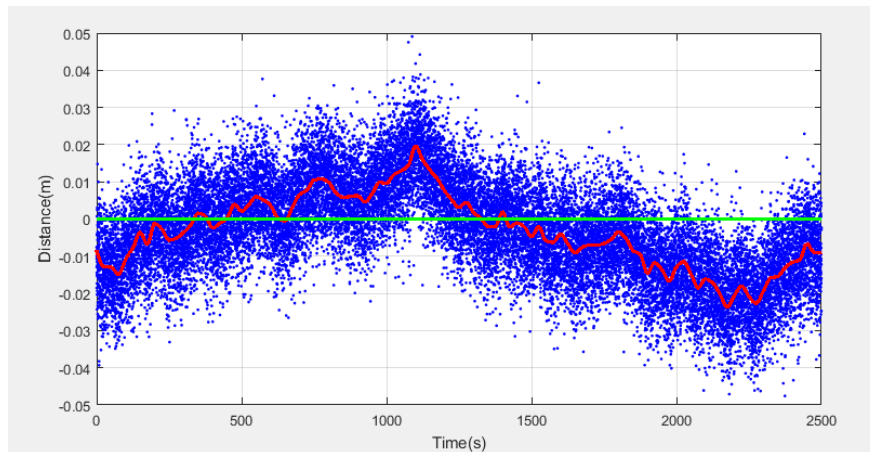

Fig. 15 **Sample Piksi error signal model, including slow varying stochastic noise (red line) about the mean (green line), and white noise (blue dots) about the red line.**

IV. Results

This section contains preliminary trajectory and docking simulation results, as well as preliminary proof-of-concept modeling and testing results for the docking mechanism described in Section III.B.

A. Dynamics Simulation Results

In the baseline operational scenario, the Rendezvous phase starts with the Chaser aircraft offset from the Target by 50 ft in Y_{sep} and Z_{sep} while trailing by 200 ft in X_{sep} as shown in Fig. 1. The Chaser GN&C architecture involves a two-loop design where the outer loop takes in the relative position and velocity errors and converts them into attitude (Q_{cmd}) and throttle (δt) commands. The inner loop consists of a Proportional Integral Derivative (PID) controller for the roll, pitch, and yaw channels respectively. Here, it attempts to track the attitude commands from the outer loop in the form of attitude errors (ϕ_e, θ_e, ψ_e). Subsequently, the outputs of the inner loop are elevator (δe), aileron (δa), and rudder (δr) commands. Figure 16 is a block diagram representation of the Chaser's GN&C architecture.
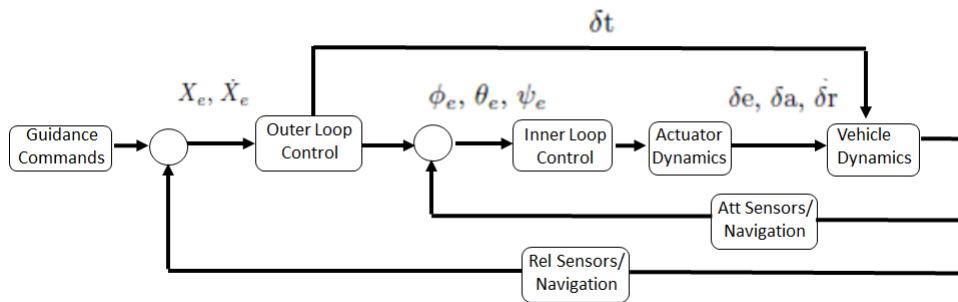
Fig. 16   Chaser GN&C architecture.

Table 6 is a representative list of system parameters along with the dispersed values used during the current trade studies phase. The nominal values are shown in the middle column and the 1σ dispersions are shown in the third column. Communication/avionics time delay and aerodynamic uncertainties appears to be the two greatest technical challenges for a successful completion of the Rendezvous and Formation Flying phase. Figure 17 shows notional results with no time delay and no uncertainties in the aerodynamics. The Chaser is fully capable of tracking the guidance commands while meeting the formation flying performance criteria.

Table 6   Representative System Parameters and Uncertainties

Parameter	Nominal	Uncertainty (1 σ)
CDGPS bias (time varying), m	0	0.02
CDGPS noise, m	0	0.003
Accelometer noise, m/s^2	0	0.002
Accelometer bias, m/s^2	0	2.943e-4
Initial attitude misalignment, deg	0	1.5
Gyro drift, rad/s	0	2.67e-5
IMU misalignment, deg	0	1.5
Time delay, ms	125	50
CG offset, m	0	0.0033
Moments of Inertia, %	0	3
Freestream aerodynamics, %	0	10
Proximity aerodynamics, %	0	10

B. Docking Mechanism Modeling and Testing Results

Explorative studies of the docking mechanism shown in Fig. 13 were performed both computationally and experimentally. Computational studies were performed using the Constrained Direct Iterative Surface Curvature (CDISC) design method [20] with the Panel Method Ames Research Center (PMARC) solver [21, 22] and the
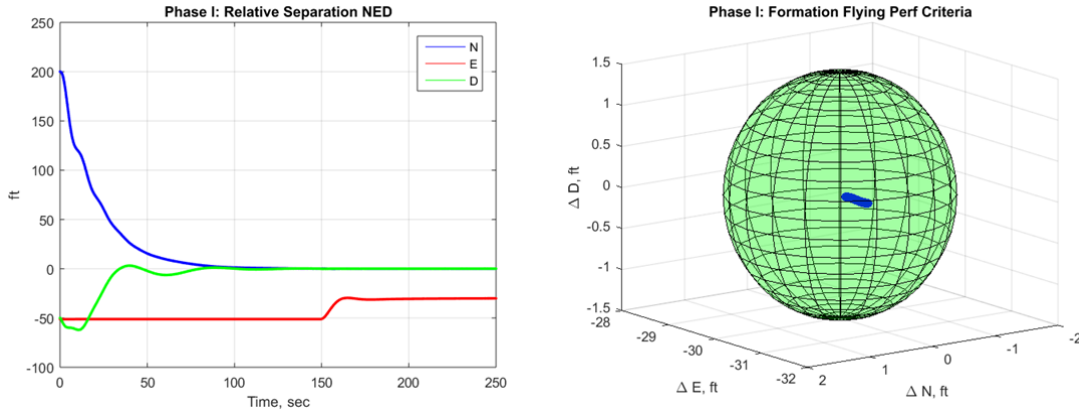
Fig. 17 Nominal results for the Rendezvous and Formation Flying phase of the CONOPS.

FlightStream unstructured vorticity surface solver [23]. Experimental work included fabrication and bench testing of small prototype linking hardware and fabrication and wind tunnel testing of larger hardware.

With the ultimate target of the autonomous wingtip docking CONOPS being a system of aircraft for HALE application, CDISC and PMARC were used to simulate a notional wing of constant chord and aspect ratio of 23.0 with inboard and outboard 30%-chord flaperons each at 50%-span length. Specifically, a comparison of the lift produced by a baseline wing without deflections was performed relative to the same wing geometry with the outboard flaperon deflected positively (upward) and the inboard flaperon deflected negatively (downward) in order to completely unload the wingtip while maintaining a total C_L of 1.0. The resulting lift distributions are presented in Fig. 18, where C_l is shown for the baseline wing configuration in black and for the deflected wing configuration in blue. This simple example suggests it is possible to move the wingtip trailing edge vortex inboard while still maintaining the integrated lift of the main wing.
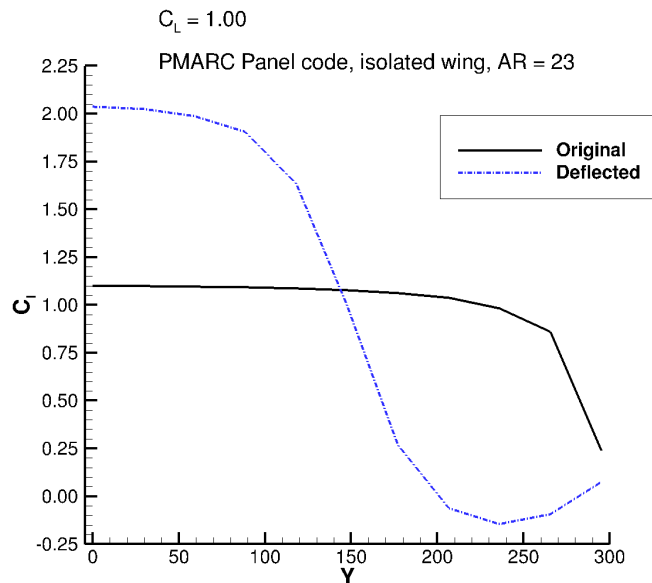

Fig. 18 Panel code results for wingtip vortex reduction concept. The black line represents the nominal wing lift distribution, and the dashed blue line is the lift distribution used to translate the wingtip vortex inboard of the tip.

A second computational investigation was performed using FlightStream, for which a candidate HALE vehicle geometry was created that included several outboard wing sections of variable twist capable of smoothly modifying the

outboard wing lift distribution. The outer-mold-line (OML) of this vehicle is shown in Fig. 19, and the outboard wing sections available for twist are illustrated by the shaded color. A qualitative study was performed using FlightStream where two of these geometries were simulated in close proximity as the wingtips approached. The simulations included variation in direction of approach (from below, from above, from behind) and total twist of the outboard wing section (-15°to +15°), with every case using a fixed angle-of-attack of 4.5°. The flow solution for a single aircraft geometry is shown in Fig. 20, where the surface is colored by vorticity contours and streamlines are rendered leaving the trailing edge of the lifting surfaces.
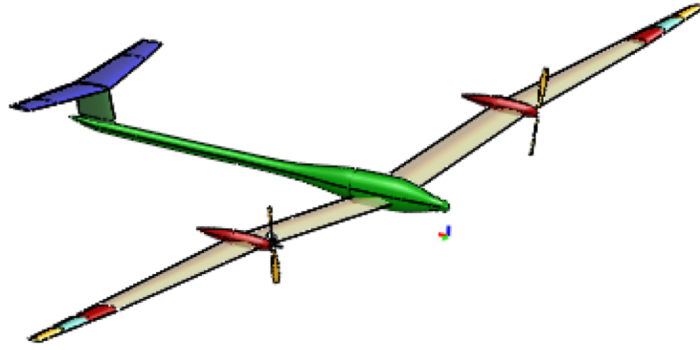

Fig. 19   Notional HALE vehicle concept geometry with outboard wing sections with customizable twist used to investigate techniques for moving the wingtip vortex inboard for wingtip docking. These wing sections are multi-colored for illustrative purposes.
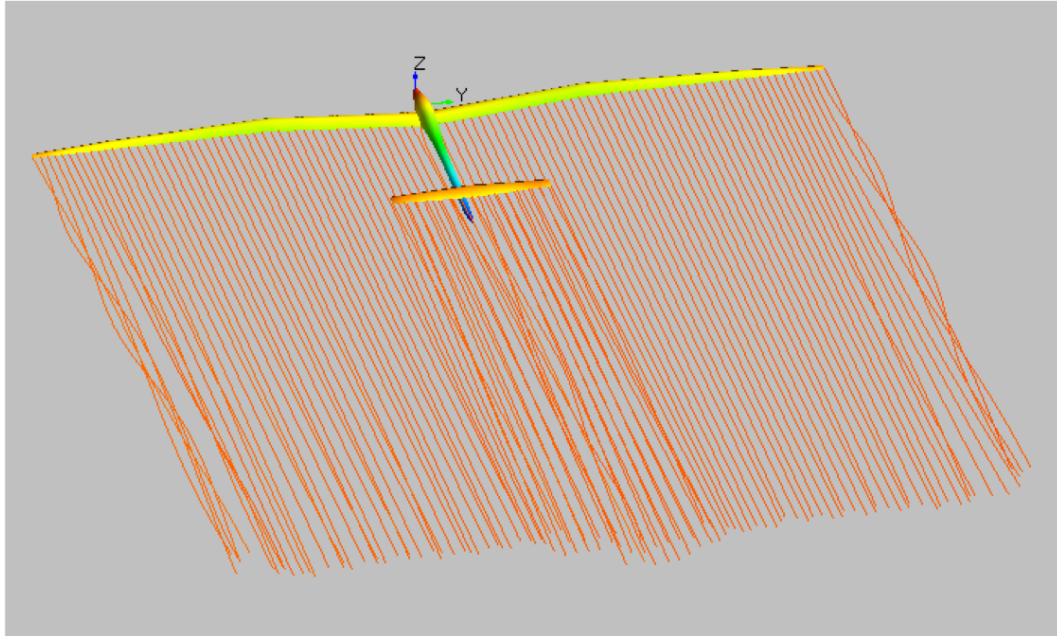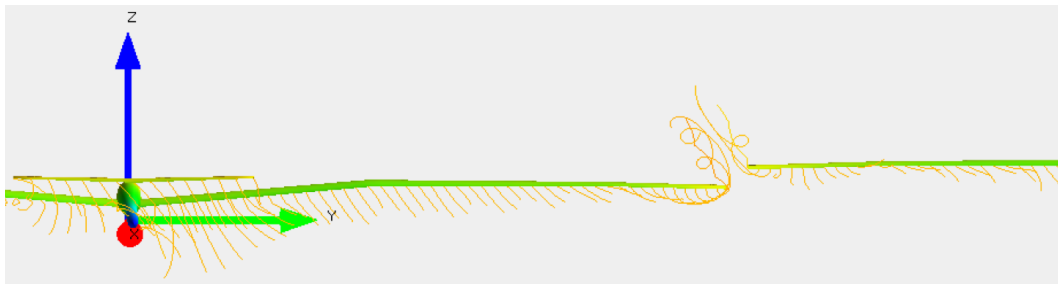

Fig. 20   FlightStream solution for a single aircraft at 4.5°angle-of-attack.

By comparing results for each of the solutions across the approach direction and control surface deflections trade space, it became clear that there is opportunity to devise an approach and outboard twist distribution that offers more-favorable aerodynamic interaction for approach and wingtip engagement. Specifically, two primary considerations became apparent: the level of aerodynamic interaction between each wingtip vortex and the assumed directionality of

the twist-induced lift. For example, the solution shown in Fig. 21 is for the case where the Chaser aircraft approaches the Target aircraft from below and both the Chaser and Target aircraft outboard wing sections are twisted to -15°, effectively moving the wingtip vortex significantly inboard. In this case, by inspecting the streamlines, one finds that there is little interaction between the two wingtip vortices, thereby increasing the probability of a successful engagement. On the other hand, the solution shown in Fig. 22 is for the case where the Chaser aircraft approaches the Target from above and both the Chaser and Target aircraft outboard wing sections are twisted to +15°, effectively strengthening the wingtip vortex. In this case, examining the streamlines suggests that although there is considerable interaction between the competing wingtip vortices, the effect of the interaction may serve to pull the airplanes together through the effective lift distribution and induced roll at very close proximity, where the separate aircraft effectively yield a single, combined lifting surface. This investigation using FlightStream warrants follow-on quantitative analysis in conjunction with the aerodynamic studies discussed in Section III.A.
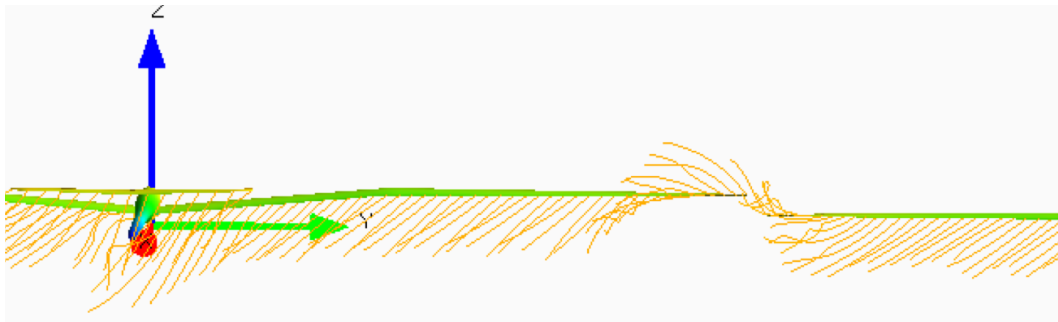

Fig. 21   FlightStream solution for two aircraft at 4.5°angle-of-attack with the Chaser aircraft approaching the Target aircraft from below. The outboard wing sections of both the Chaser and Target aircraft are twisted to -15°.

Fig. 22   FlightStream solution for two aircraft at 4.5°angle-of-attack with the Chaser aircraft approaching the Target aircraft from above. The outboard wing sections of both the Chaser and Target aircraft are twisted to +15°.

An experimental investigation of the docking mechanism was conducted to evaluate its preliminary feasibility. Specifically, the two primary aims of the experimental investigation included: assessing the feasibility of moving the wingtip vortices inboard of the wingtip using deflection of the outboard section of the wing; and investigating the operational feasibility of the linkage mechanism concept itself. The first experiment consisted of benchtop testing of the stiffened cable and hook approach, where Figs. 23 and 24 show several variants of linking mechanism hardware employing trailing cables or cable loops and hooks that were fabricated and bench tested. This bench testing included testing small scale flat "wings" so that they are automatically linked and the wingtips pulled together. These simple tests showed the preliminary viability of the cable-hook docking approach and that wind tunnel testing was warranted.

A larger-scale prototype of the docking mechanism was fabricated along with a set of two wings for proof-of-concept testing in the NASA Langley Research Center Vertical Spin Tunnel (VST) wind tunnel [24]. The fabricated wings are shown in Fig. 25, where each has two 5 ft actuated trailing edge sections. These wings were mounted to roll carts at the VST, so that technicians could manually engage the two wingtips in the VST flowfield. A smoke wand was also employed to visualize the wingtip vortices and their interaction as the wingtips approached. Video was collected
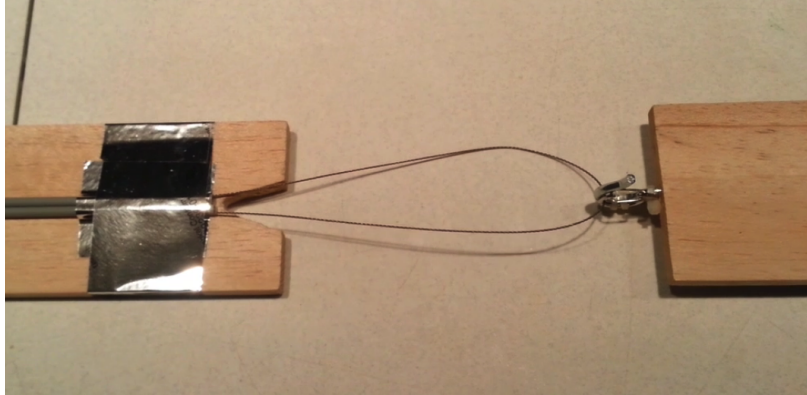
Fig. 23   Benchtop test of the wingtip docking mechanism relying on a spring-retraced, stiffened cable and capture hook. Note that this is a still image from a video of the test.

Fig. 24   Benchtop test of the wingtip docking mechanism, where the wing shown in the right is swung in and captured by the wing shown on the left. Upon engagement, a spring-loaded cable system retracts the cable until a physical dock is achieved. Note that this is a still image from a video of the test.

demonstrating the significant impact that unloading the outboard sections of the wings had on the docking mechanism tether. A still image from the collected video is shown in Fig. 26, depicting the smoke wand illuminating the Target aircraft wingtip vortex and the orientation of the tether and drogue bulb. With both outboard wing sections loaded, it was nearly impossible to engage the tether with the capture hook, as the tether and small drogue bulb would quickly get captured in the Chaser aircraft's wingtip vortex. When the Chaser aircraft outboard wing section was unloaded, there was no observed interaction of the wingtip vortices with the tether and drogue bulb. Hence, this qualitative test points to the viability of the wingtip vortex reduction concept studied in this paper.

V. Summary and Future Work

Formation flight has proven that advantageous aerodynamic coupling of multi-aircraft systems can lead to mission-level performance benefits. In this paper, some of the technical challenges associated with extending formation flight to the limit of autonomous in-air wingtip docking were investigated. This study included: development of a docking CONOPS and related vehicle and mission constraints; aerodynamic analysis using both a lower order wake model representation and also Euler CFD simulations to characterize the aerodynamic coupling as a result of offset distances; development of a dynamics simulation framework to study the integrated effects of dynamics, aerodynamics, sensors, and control laws for autonomously docking two aircraft; and proof-of-concept analysis and testing for a linkage mechanism for wingtip docking. The tools developed in support of this work leveraged the 5.5% scale NASA GTM model. Even though this configuration represents a typical transonic airliner, the relatively large quantity of publically-available vehicle data made it suitable for benchmarking purposes.

Fig. 25 Wings fabricated for wind tunnel testing of the docking mechanism. Note that each of the 10 ft span wings have inboard and outboard actuated ailerons used to selectively unload the wings during testing.
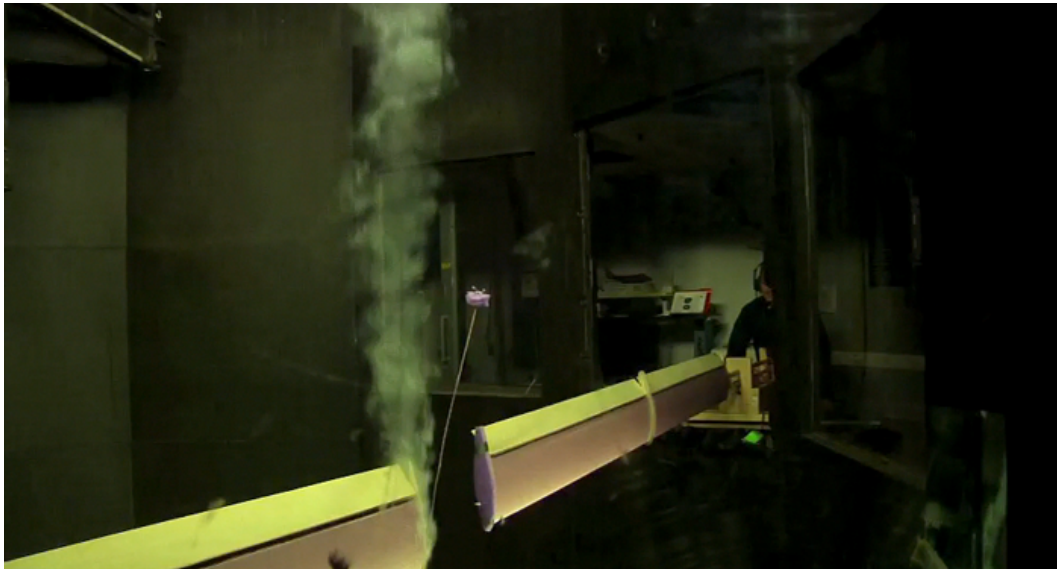
Fig. 26 Demonstration of the aerodynamic interaction associated with the docking mechanism concept, where in this image the Chaser aircraft wing (right side) outboard section is unloaded and is approaching the Target aicraft wing (left side) while fully-loaded. Note that this is a still image from a video of the test.

This work was an incubation activity to determine the feasibility of autonomous wingtip docking for range extension applications. As such, considerably more work remains to determine ultimate feasibility. Specifically, structural and aeroelastic effects must be integrated into the tools described in this paper , and future applications will include vehicles designed for linked flight and relevant long-range applications, such as HALE flight. Additionally, the aerodynamic work completed here will be leveraged directly with the dynamics simulations in order to improve the lower order

wake modeling approach used in prior work. The dynamics simulation framework will be used to perform more expansive trade studies on mission and vehicle parameters of interest; in particular, refinements of the docking CONOPS constraints will be pursued. Finally, the linking mechanism concept discussed in this paper will be refined with further analysis and testing and for potential scalability to suit mission and vehicle needs for a variety of aircraft concepts.

Acknowledgments

References

[1] Latimer-Needham, C. H., *Apparatus for Aircraft-Refueling in Flight and Aircraft-Towing*, Flight Refueling Ltd., Patent No. 2716527, 1955.

[2] Leisy, C. J., *Aircraft Interconnecting Mechanism*, Boeing Airplane Company, Patent No. 2663523, 1953.

[3] Newman, J., "X-47B Passes Unmanned Refueling Test," Accessed May 28, 2018. URL http://navalaviationnews.navylive.dodlive.mil/2015/07/29/x-47b-passes-unmanned-refueling-test/.

[4] Warwick, G., "KQ-X - Yes, That Is How They Do It," Accessed May 2018, 2018. URL http://aviationweek.com/blog/kq-x-yes-how-they-do-it.

[5] Wilson, D. B., Goktogan, A. H., and Sukkarieh, S., "Guidance and Navigation for UAV Airborne Docking," *Robotics: Science and Systems XI*, Rome, Italy, 2015.

[6] Anderson, C., "Project Tip-Tow," *Air Force Magazine*, 2012.

[7] Devuono, A. J., and Shearer, C. M., "Flight Dynamic Response of HALE Aircraft to KC-135 Flowfield," *AIAA Atmosopheric Flight Mechanics Conference and Exhibit*, AIAA 2008-6710, Honolulu, HI, 2008.

[8] Jordan, T., Langford, W., Belcastro, C., Foster, J., Shah, G., Howland, G., and Kidd, R., "Development of a Dynamically Scaled Generic Transport Model Testbed for Flight Research Experiments," *AUVSI Unmanned Systems North America 2004 Symposium and Exhibition*, Anaheim, CA, 2004.

[9] Grauer, J. A., and Morelli, E. A., "Generic Global Aerodynamic Model for Aircraft," *Journal of Aircraft*, Vol. 52, No. 1, 2015.

[10] Binetti, P., Ariyur, K. B., Krstic, M., and Bernelli, F., "Formation Flight Optimization using Extremum Seeking Feedback," *AIAA Journal of Guidance, Control, and Dynamics*, Vol. 26, No. 1, 2003.

[11] Aftosmis, M., "Cart3D Resource Website," Accessed May 28, 2018. URL https://www.nas.nasa.gov/publications/software/docs/cart3d/index.html.

[12] National Oceanic and Atmospheric Administration, National Aeronautics and Space Administration, United States Air Force, "U.S. Standard Atmosphere, 1976," Tech. rep., 1976.

[13] Cuji, E., "Analysis of Linked Aircraft Aerodynamics and Flight Dynamics," Ph.D. thesis, Cornell University, 2011.

[14] "SideArm Prototype Catches Full-Size Unmanned Aerial System Flying at Full Speed," Accessed May 2018, 2018. URL https://www.darpa.mil/news-events/2017-02-06.

[15] "Gremlins Takes Flight to Provide Air-Recoverable Unmanned Air Systems," Accessed May 29, 2018. URL https://www.darpa.mil/news-events/2016-03-31.

[16] Mohiuddin, S., and Psiaki, M., "High-Altitude Satellite Relative Navigation Using Carrier-Phase Differential Global Positioning System Techniques," *Journal of Spacecraft and Rockets*, Vol. 30, No. 5, 2007.

[17] Leung, S., and Montebruck, O., "Real-Time Navigation of Formation-Flying Spacecraft using Global-Positioning-System Measurements," *Journal of Guidance, Control, and Dynamics*, Vol. 28, No. 2, 2005.

[18] Pei, J., Murchison, L., BenShabat, A., Stewart, V., Rosenthal, J., Follman, J., Banchy, M., Sellers, D., Elandt, R., Elliott, D. S., Choueiri, M., Peck, M., and Finch, M., "Ground Demonstration on the Autonomous Docking of Two 3U Cubesats Using a Novel Permanent-Magnet Docking Mechanism," *AIAA SciTech Forum*, AIAA 2017-0849, Grapevine, TX, 2017.

[19] *Piksi DataSheet*, SwiftNav, June 2013.

[20] Campbell, R. L., "Efficient Viscous Design of Realistic Aircraft Configurations," *AIAA Fluid Dynamics Conference*, AIAA 1998-2539, Albuquerque, NM, 1998.

[21] Ashby, D. L., Dudley, M. R., and Iguchi, S. K., "Development and Validation of an Advanced Low-Order Panel Method," Tech. rep., NASA TM-101024, Oct. 1988.

[22] Ashby, D. L., Dudley, M. R., Iguchi, S. K., Browne, L., and Katz, J., "Potential Flow Theory and Operation Guide for the Panel Code PMARC," Tech. rep., NASA TM-102851, Nov. 1995.

[23] Research in Flight, "FlightStream," Accessed May 29, 2018. URL https://www.researchinflight.com/index.html.

[24] *Langley Research Center's 20-Foot Vertical Spin Tunnel*, National Aeronautics and Space Administration, NP-2008-11-122-LaRC, 2008.